CHARACTERISING AND MODELLING TOOL-PLY FRICTION OF VISCOUS TEXTILE COMPOSITES

Philip Harrison[1*], Rene ten Thije[2], Remko Akkerman[2], Andrew C. Long[3]

*Corresponding author: **Philip.harriso@Glasgow.ac.uk**

[1]Department of Mechanical Engineering, University of Glasgow, Glasgow G12 8QQ, Scotland

[2]University of Twente, PO Box 217, NL-7500AE Enschede, The Netherlands

[3]University of Nottingham, Faculty of Engineering, Division of Materials, Mechanics & Structures, University Park, Nottingham NG7 2RD, UK

Keywords: Friction, Viscous Textile Composite

Abstract

The paper describes two experimental methods for measuring the tool-ply friction behaviour of impregnated thermoplastic textile composites. These include the pull-through and pull-out tests on the one hand and experiments conducted using a commercial rheometer using custom designed platens on the other. Results from the techniques are compared and the relative advantages and disadvantages are discussed. A simple procedure to determine parameters in a so-called master curve, an empirical model relating the friction coefficient to normal pressure, velocity and temperature is demonstrated. The model is convenient for implementation in a numerical code. A predictive meso-scale model is also described that incorporates parameters such as fabric architecture, tow geometry and matrix viscosity. The model is based on lubrication theory and can predict steady state friction over a broad range on conditions. Significantly, unlike previous attempts to model tool-ply friction using a meso-structural approach, there is no need to experimentally determine the lubrication film thickness as this is an output of the model. Meso-scale model predictions are compared with predictions from the master equation and experimental data.

1 INTRODUCTION

Press forming of thermoplastic textile composites is potentially a fast and efficient method of production. However, while stretch-forming and deep-drawing of sheet metal [1] are today relatively well understood processes supported by sophisticated Computer Aided Engineering (CAE) tools [2] the same cannot yet be said for textile composites. As such a large research effort is underway to create equivalent CAE tools for these materials. The manufacture of textile composite components of potentially complex double curvature geometries involves a forming stage in which dry or pre-impregnated reinforcement takes the required shape through deep-drawing. Wrinkling of the sheet during forming is an unwanted defect and can be inhibited via in-plane tension induced in the sheet using a blank-holder [1-5]. Friction occurring between the composite material and metal tooling during forming imparts tensile stresses in the sheet. These tensile stresses help counteract the compressive stresses generated by material deformation that are responsible for wrinkling.

Several experimental methods have been employed to investigate the inter-ply [6-10] and tool-ply [10-18] friction behaviour of impregnated textile [7, 9-11, 15-20] and uniaxial [6-8, 21] continuous fibre reinforced composites. A heated metal sled drawn across a heated textile

composite sheet was used by Murtagh et al. [21]. An early investigation by Scherer and Friedrich [8] reported a pull-out test which could be used to characterise both tool-ply and ply-ply friction over a range of temperatures. Similar pull-out designs of varying levels of sophistication and accuracy have been used in subsequent investigations [6, 8-11, 16, 17, 20-23]. Wilks developed a modified version of the pull-out test, a so-called pull-through test, that benefited from a constant contact area between specimen and platens during the test [20]. The platens were electrically heated and the rig housed entirely inside an environmental chamber allowing more accurate temperature control of the specimen during the test [15, 18, 19]. A similar pull-through design was later used by Gorczyca et al. [14, 24-26], though in this case without the use of an environmental chamber. Notably, investigations by Gorczyca et al. [14, 24] aimed to reproduce conditions similar to those experienced during actual forming operations and employed the technique of heating the preform and tooling to different temperatures from each other before testing. More recently commercial rheometers have been adapted to perform friction measurements [15, 18, 19, 27] . The technique, which is reported in Section 3.2 of this paper provides a fast and efficient method to generate experimental data, though is limited to relatively low pressures and velocities far removed from actual processing conditions. One of the aims of this paper is to examine how useful such experiments are in predicting more realistic friction boundary conditions.

Gorczyca et al. [24] summarise some of the different materials and test conditions that have been investigated and reported in the literature. Materials have included: AS4/PEEK [6], carbon/PP [8] and carbon/PEEK APC-2 unidirection composites [21] as well as both balanced and unbalanced pre-consolidated glass/PP twill woven composites [3, 10, 11, 15, 16, 18, 19, 23], glass/PP satin weave composites [28] and glass/PP plain weave composites [14, 24, 29] . Force versus displacement data produced by constant displacement rate tests typically follow a generic form characterised by an initial peak force, rapidly falling to a lower steady state value, irrespective of the material under consideration [6, 10, 15-19][1]. Thus, two friction coefficients can usually be determined corresponding to a peak and steady state response. An exception to this occurs when the displacement rate is very low (e.g. 10mm/min) [18] or the temperature is high [6, 10], under these conditions the peak in the force curve decreases and in some cases can completely disappear.

Several factors, listed below, have been investigated to determine their effect on the coefficient of friction between tool and composite including: normal pressure [11, 14-25], draw velocity [11, 14-25], tool-material [21], tool-temperature [11, 14-25], fabric temperature prior to forming [13, 14, 30], fabric orientation [6, 8, 13, 14, 21, 30], type of release agent [21] and cooling conditions [10]. Certain factors have been found to be much more important than others. Gorczyca et al. [14, 24, 25] list velocity, tool temperature and normal pressure as the most influential factors in their investigation while fabric temperature prior to forming and fabric orientation seem to have only a minor effect. In contrast, relative ply orientation has a significant effect for uniaxial continuous fibre reinforced composites [7, 8]. Murtagh et al. [21] found release agents had a significant effect and changing the tool material from metal to rubber also caused a large increase in friction. Lebrun et al. [10] investigated effects arising from the significant difference between melting temperature upon heating and re-crystallisation temperature during cooling. Several studies confirm that the coefficient of friction is inversely proportional to normal pressure and directly proportional to velocity [10, 11, 14, 15, 17-19, 21, 24, 25] . Increasing temperature was unexpectedly found to increase tool-ply friction in two studies [10, 21] an effect explained by the action of Coulomb type friction between fibres and metal [10], but more generally has been observed to decrease the friction coefficient due to the associated reduction in matrix viscosity [10, 11, 14, 16-19, 24, 25].

[1] Controlled force-displacement tests show a yield stress rather than a peak [Scherer & Freidrich (1991); Morris & Sun (1994)].

A purely empirical approach to modelling friction was presented by Morris and Sun [6] who determined a power-law relationship between steady-state friction, slip velocity and temperature. Murtagh et al. [22] assumed a lubricating layer in a first modelling attempt to relate friction to the micro-mechanics of the sliding process. Wilks et al. [23] proposed another simple model including a combination of both Coulomb friction and hydrodynamic lubrication. In this work both the film thickness and friction coefficient were used as fitting parameters for the model. Their model was later modified to account for the surface area of the viscous and reinforcement fractions [31]

$$\tau = \eta\,\dot{\gamma} + \phi\,\mu_c\,P_N \qquad (1)$$

where η is the viscosity of the matrix, $\dot{\gamma}$ is the shear strain rate, μ_c is the Coulomb friction coefficient (assumed equal to 0.3), and P_N is the normal pressure. $\phi = A_f / A$, is the ratio of fibres in contact with the tool to the overall platen area, A. The shear strain rate is simply the crosshead displacement rate divided by the thickness of the molten polymer film separating the reinforcement fibres and the tooling. They used a series of optical micrographs to measure the film thickness from un-tested composite samples, giving an average value of 0.07mm. Further micrographs were analysed from tested samples to determine the proportion of fibres in contact with the platen. Their model compared well with experimental data generated using the pull-through test designed by Wilks [20].

The clear dependence of friction on normal force, displacement rate and matrix viscosity prompted Chow [28] to propose the use of a Stribeck curve to interpret experimental data, an approach adopted since by others [11, 13, 14, 16-18, 28, 30]. A Stribeck Curve is a plot of the coefficient of friction μ as a function of the multiple (Hersey number), $H = \eta v/P$, where η is the viscosity of the lubricating fluid layer, v is the velocity and where P was originally defined as the normal force per unit width (for bearings) [32, 33], in which case H is a dimensionless number, but has also been used since as the normal force [13-15, 34] or the normal pressure [11, 16]. A typical Stribeck Curve is shown in Fig 1 which shows three distinct regions corresponding to Boundary Lubrication, Elasto-Hydrodynamic Lubrication and Hydrodynamic or full-film lubrication.

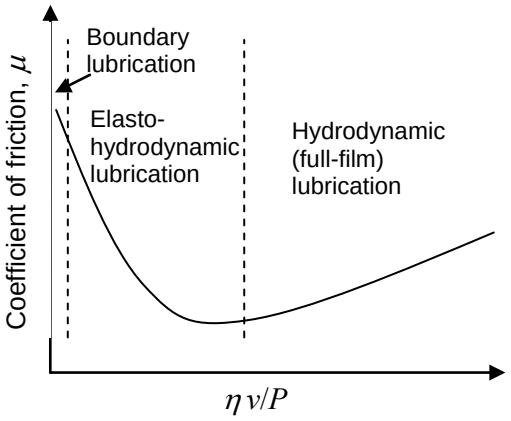

Fig 1. The variation in frictional drag (expressed as the coefficient of friction, μ) with the quantity $\eta v/P$: the Stribeck curve. (From Hutchings [32])

In this paper P is used to indicate normal pressure as comparisons shown later in this paper, involve data from experiments employing testing platens of different areas, and obtained over a range of normal forces. Chow [28] originally proposed a similar model to Eq (1), assuming the friction behaviour belonged to the Elasto-hydrodynamic region shown in Fig 1. However, investigations on a plain weave glass/PP fabric [14] indicated that friction behaviour for this particular material fell into the Full-Film lubrication region of Fig 1. The steady increase in friction with increasing Hersey number allowed them to propose a model including a linear relationship between the steady state friction coefficient and the Hersey number. However, to account for changes in temperature they had to include a linear shifting term:

$$\mu = 6.12H + 0.27 - S_{tt} \quad (2)$$

where μ is the friction coefficient, H is the Hersey number (defined with normal force as the denominator) and S_{tt} is the shift factor based on the tool temperature. So far all the models reviewed, with the exception of [6] who used a purely empirical approach, have required an estimate of the lubricating film thickness based on experimental measurements in order to determine the shear rate and from there the viscosity of the non-Newtonian fluid film. Recently a meso-scale model has been proposed based on the fabric architecture [11, 16, 17, 19] and on the fluid mechanics occurring within the lubricating film. The most interesting feature of this model is that the film thickness is an output rather than an input of the model. The model is described later in this paper in and its predictions compared with experimental results in Section 5.

Regarding numerical work, attempts to include Eq (2) into finite element simulations have been published [13, 14, 30]. A simple friction rig scenario was modelled in [30] and rate dependence of the friction coefficient was reproduced. The work was developed further in [13, 14] to include normal force and tool temperature dependence. Simulations of the friction tool were correct to within less than 8 percent. Thermo-stamping simulations were also conducted and results analysed in terms of the punch reaction force. Generally the expected trends were observed though the constitutive model used to represent the fabric was also found to influence results.

2 MATERIAL

A balanced 2x2 twill weave pre-consolidated thermoplastic textile composite, Vetrotex Twintex®, consisting of commingled E-glass and polypropylene (PP) yarns has been tested. It has an areal density of 710gm^{-2}, a yarn width of 5mm in both warp and weft directions, a nominal thickness of 0.5 mm and a fully consolidated fibre volume fraction of 0.35. The glass fibre diameter is 16 microns [35]. The form of the upper surface of the tows affects the lubrication flow during sliding friction. Thus, tow geometry is one of the inputs in the meso-scale model and can be parameterized using a polynomial equation. The length dimensions of the longitudinal and transverse tows together with the coefficients of the quadratic used to describe the surface profile of the yarns are given in Table 1. The basic structure assumed in the model is shown in Fig 2 together with a photograph of the pre-consolidated composite in Fig 2.

Table 1. Input values for the meso-scale model required to predict the empirical results.

Parameter	Value
Transverse bundle length (mm)	5.0 *mm*
Transverse bundle approximation	$y = 8 \cdot x^2$
Longitudinal bundle length (mm)	10.0 *mm*
Longitudinal bundle approximation	$y = 16 \cdot x^2$

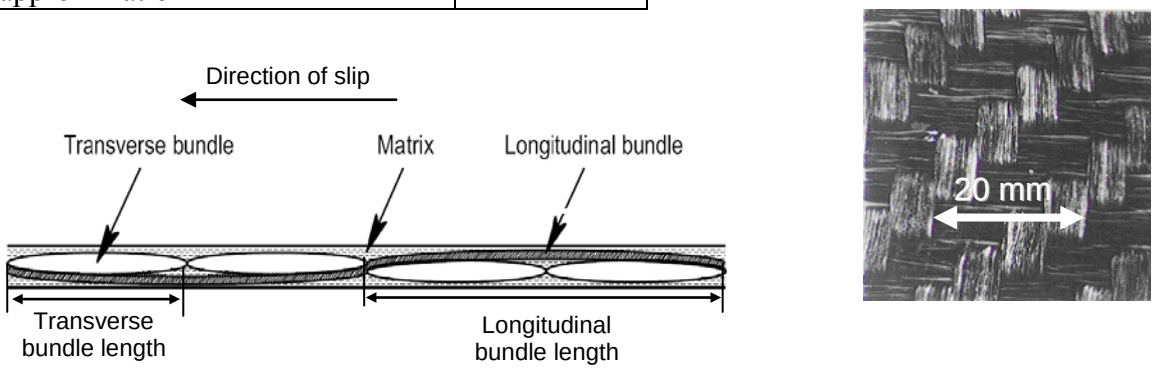

Fig 2. Left: Schematic cross section of a Twintex ply. Right: 2 x 2 Twintex® glass-polypropylene preconsolidated sheet.

3 EXPERIMENTAL METHODS

In this investigation data collected using two generic experimental techniques has been analysed. These include pull-out [23] and pull-though [18, 20] tests on the one hand and rotational measurements using a commercial rheometer [18] on the other. Hands-on experience with the different techniques is useful when discussing their relative merits; the advantage of the rheometer lies in the higher rate at which test results can be produced when compared to more traditional pull-out and pull-though methods and also the greater temperature control afforded by the much smaller environmental chamber. The disadvantage is that the experimental conditions obtainable using the rheometer (normal pressure, P, and velocity, v) are lower than can be expected in typical forming situations (P up to ~ 1000KPa and v up to ~ 5000 mm/min [30]) and so any results have to be extrapolated to the relevant processing conditions. The low velocities accessible using the rheometer also mean that only steady state friction behaviour can be measured as the peak in a typical force versus displacement typically disappears at low slip velocities [18]. Measurements using the pull-through set-up showed that the temperature at the bottom of the environmental chamber could be up to 30^{o}C lower than at the top of the chamber, even when using the convection fan. For slow rates this was not too problematic as the electrically heated platens had sufficient time to heat the specimens to the correct temperature as the composite material moved against the metal. At higher rates the heating time decreased causing large variations in the higher rate data. Thus, the time-dependent heating of samples as they are drawn between the platens is found to be a cause of variability and can be expected to be even more of an issue for test rigs not housed within an environmental chamber. The test method was found typically to require between 40-60 minutes for each test making collection of a large amount of data a laborious and costly process and test repeatability was rather poor.

3.1 Pull-out rig

The first set of experimental data used in this investigation was collected using a pull-out rig developed by Murtagh et al. [22] in an investigation conducted by Wilks et al. [23]. A schematic of the set-up is shown in Fig 3. The technique involves pulling a steel shim from between two layers of composite sheet clamped by a steel bar on three sides. A normal load was applied by two heated platens, driven by a Dartec 100kN universal testing machine. The area of the two heated platens was 0.012m^2. Once the desired temperature was reached, the shim was pulled out by a lead screw driven by a variable DC permanent magnet motor. A 2.2kN load cell was placed between the lead screw and the clamping device for the steel shim to measure the force required to withdraw the shim. Displacement of the steel shim was measured by a +/- 25mm stroke linear variable differential transformer mounted horizontally. Testing conditions include temperatures of 180, 200 and 220^{o}C, normal pressures of 80kPa to 2.8MPa and pull-out velocities of 0.5, 0.8 and 1.2 mms^{-1}. Starting at 0.5 mms^{-1}, all three velocities occurred during a single test. Once the pull-out force became constant the velocity was rapidly increased to 0.8 mms^{-1} and again to 1.2 mms^{-1}.

3.2 Pull-through rig

Wilks [20] later designed a pull-through rig, so-called to distinguish it from similar pull-out designs [11, 16, 21, 23]. A photograph of the rig is shown in Fig 4 together with a schematic of the top view of the rig. The rig consists of a primary steel frame approximately 300 x 200 mm with two steel platens, 175 x 25 x 6 mm constituting the top section of the frame. A secondary specimen frame clamps the perimeter region of the sample and is connected to the load cell at it upper point. The sample is the same size as the outer perimeter of the specimen frame which is guided in its motion by grooves milled into the faces of the steel platens. The specimen frame effectively pulls the clamped sample between the two steel platens which apply a normal pressure to the front and back surfaces of the sample. The bottom edge of each platen is milled to prevent snagging of the sample as it is drawn through the platens. The contact area between platen and material is 89 x 63 mm (area = 5607mm^2). Two 50 W cartridge heaters heat each platen to the test temperature, which is regulated by a feedback loop using two K-type thermocouples. The normal pressure on the

platens is provided by four springs. In order to heat material initially outside of the heated platens, the entire rig is placed in a Hounsfield Environment Chamber (fan-assisted oven) and heated to the same temperature as the platens. The intention is that the temperature of both the oven and platens should be identical and testing is as close to isothermal as possible. The specimen frame is connected to the crosshead of a PC-controlled Hounsfield H25k-S Universal testing Machine, fitted with a 2.5 kN load cell. The test specimens can only be tested in a 0° or 90° configuration otherwise the frame is unable to clamp the specimen securely enough to prevent significant distortion of the textile composite during testing. Each experiment was conducted at least three times.

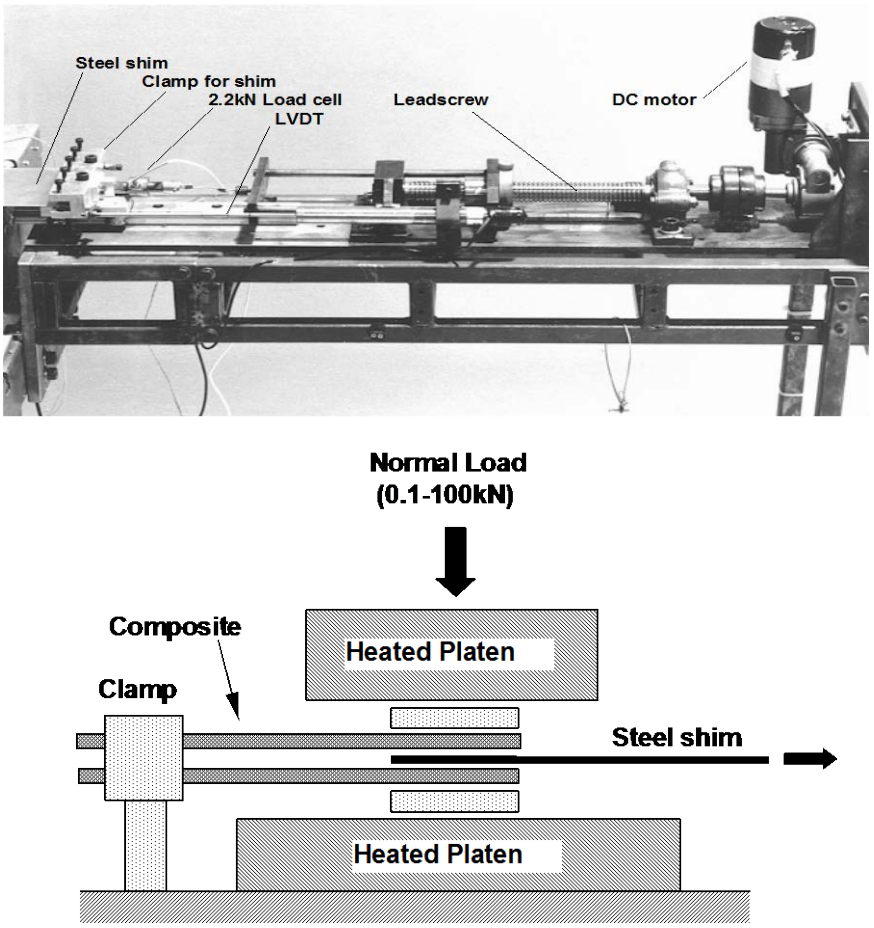

Fig 3. Top: Photograph of experimental set-up. Bottom: Illustration of steel shim being pulled out from between two heated composite plies to which a normal load is applied.

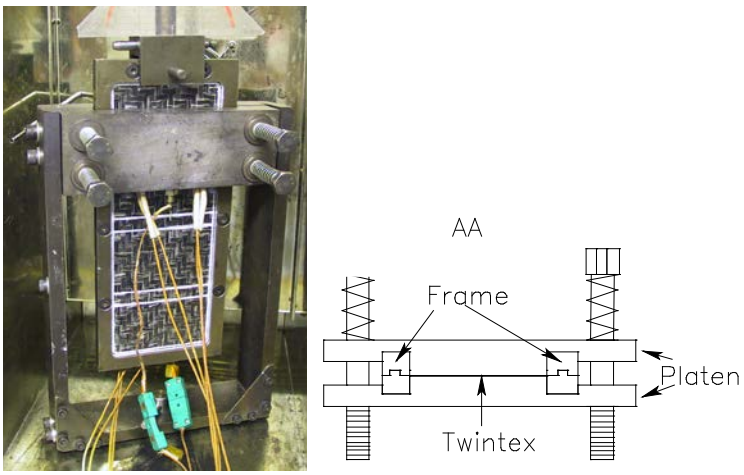

Fig 4. Pull-through rig. Left: Photo of pull through rig in oven. Right: Schematic of rig viewed from above.

Typical results from a pull-through experiment performed at a normal pressure of 0.012 MPa are shown in Fig 5. The temperature during each experiment was kept constant at 180°C. The force versus displacement curves show peak values followed by steady state values. Thus, both peak and steady state friction behaviours are evident and both follow the same general trends. These include increasing friction with increasing rate and decreasing friction for increasing normal force. These same trends have been reported previously for other types of Twintex [11, 14, 16, 17, 23] . In this investigation only steady state friction has been considered. The list of experimental conditions employed for pull-out (Table A1) and pull-through tests (Table A2) are given in Appendix A.

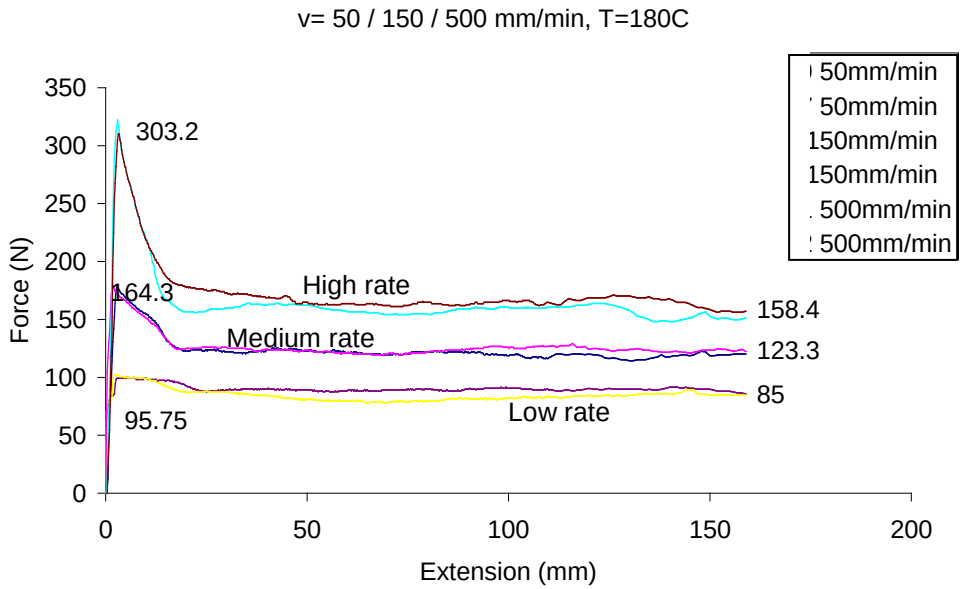

Fig 5. Typical results from the Pull-though rig tests conducted at 3 rates using a pressure of 0.012 MPa. Numbers given by the lines indicate the average peak and steady state forces recorded during the tests.

3.3 Rheometer

An alternative method of measuring friction has been employed by adapting a commercial rheometer [15, 19, 27]. Experiments were performed on a Bohlin CVOR200 Rheometer with an Extended Temperature Cell. All tests were conducted in a nitrogen atmosphere to minimize polymer degradation. The rheometer was fitted with a custom designed rig that allowed the textile composite samples to be held firmly in place during testing. The rig consisted of a pair of parallel stainless steel platens. The lower platen was a truncated cone with a diameter of 25 mm. The upper platen was a flat disk with diameter 40 mm (Fig 6). Specimens were cut appropriately (see Fig 7) and placed between the upper platen and a clamping ring (outer diameter of 40mm and inner diameter of 30mm). Four small screws were used to clamp the ring and specimen in position. The screws secured the specimen by passing through the ring and into the upper platen. The specimen was placed in the Extended Temperature Cell and heated. After the specimen reached the required temperature, the upper platen holding the specimen was positioned in the rheometer parallel with the lower platen. A normal force was set on the specimen by pressing the upper platen down against the lower platen. The value of the normal force was recorded by the computer.

Using the rheometer it was possible to generate data more efficiently than when using the pull-though and pull-out test rigs. This meant a much larger test matrix could be completed in a reasonable amount of time, presenting the possibility of generating a master curve incorporating rate, normal pressure and temperature. Formulating the master curve involves shifting the data produced under different experimental conditions such that the whole body of data can be described using a single equation. In order to do this, suitable shifting factors must be determined. The input data in the rheometer are normal force, shear stress and temperature. Experiments were performed over a range of normal forces (2.5, 10, 20, 50 and 90% of the maximum force that could be applied

by the rheometer, i.e. 19.6 N), at various imposed shear stresses (500, 1100, 2000 and 5000Pa) and for several temperatures (160, 180, 200 and 220°C). Each test was repeated three times and average results were used for data processing. It was found during experiments that normal force changed due to lateral squeeze-flow of the polymer matrix through the sample. Thus normal force was also one of the outputs from the test and was recorded continuously. Other outputs included rotation angle and time. A typical test result is shown in Fig 8 which shows angular displacement versus time for a given imposed constant torque (constant shear stress).

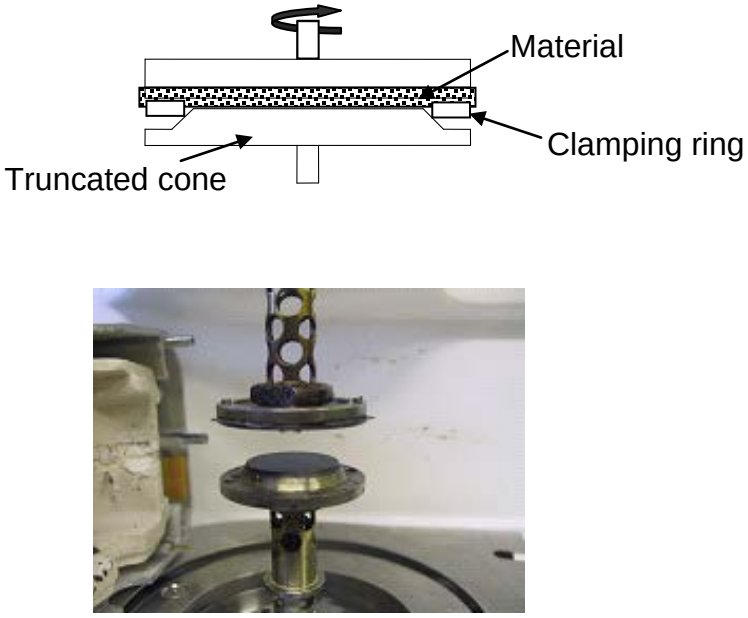

Fig. 6. Top: Side profile of custom made fixture with loaded sample. Bottom: Photograph of custom designed platens.

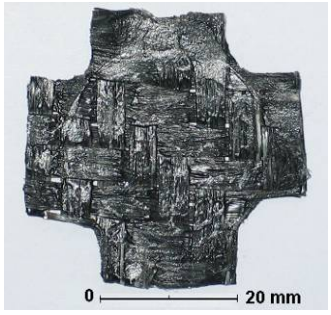

Fig. 7. Example of a test sample following testing. The arms of the specimen are fastened under the clamping ring.

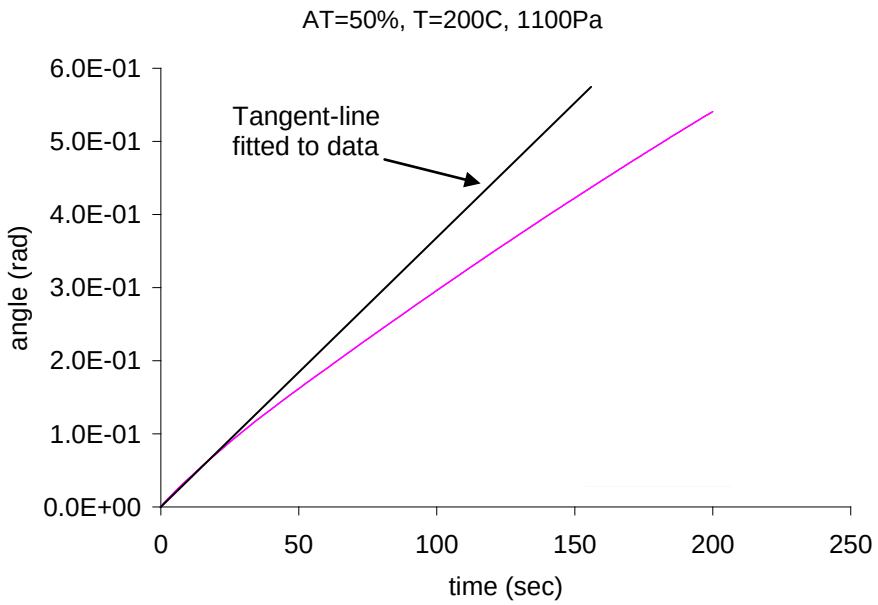

Fig 8. Output data from an individual rheometer test. The initial tangent of the experimental curve was used to determine angular shear rate.

3.4 Shifting Procedure for rheometer data

Clearly the data from the rheometer have to be adjusted for comparison with results from the pull-through and pull-out tests. The normal force, n, can be converted to normal pressure, P, by

$$P = n / A_o \tag{3}$$

where A_o is the testing area (πR^2) and R is the radius of the truncated platen (see Section 3.3). The angular velocity at any radius, r, can be converted to linear velocity (mm/s) using $v=\omega r$ where ω is the angular velocity (calculated from the initial gradient of the line shown in Fig 8) and r is the radius. The linear velocity varies from zero at $r = 0$ to a maximum at $r = R$. The weighted average linear velocity is used to process the rheometer data for comparison against pull-through tests, i.e.

$$v = \frac{2}{3}\omega R \tag{4}$$

Typical data generated by the rheometer tests at a temperature of 180°C, showing normal mass (the applied load measured in grams), m, versus linear velocity, v, for different imposed constant shear stresses are plotted in Fig 8. Similar graphs were also produced for temperatures of 160°C, 200°C and 220°C (not shown here). Trend lines were fitted through the data. Each trend line was of exponential form as in Eq (5). The average exponent, C_2, of all trend lines at different temperatures and shear stresses was found to be -1.37 with a standard deviation of 0.4. C_1 changed according to the different experimental conditions.

$$P = C_1 \cdot v^{C_2} \tag{5}$$

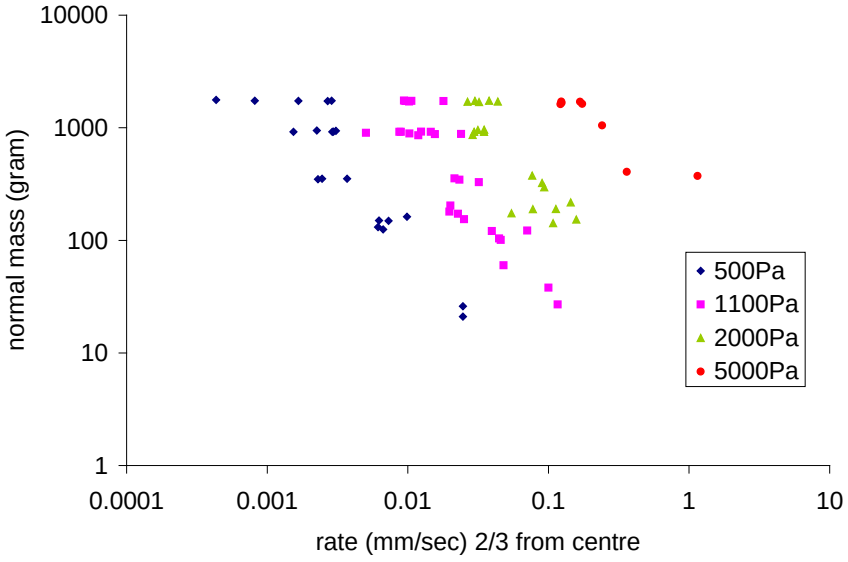

Fig. 9. Normal mass versus rate data generated for different shear stresses at 180°C.

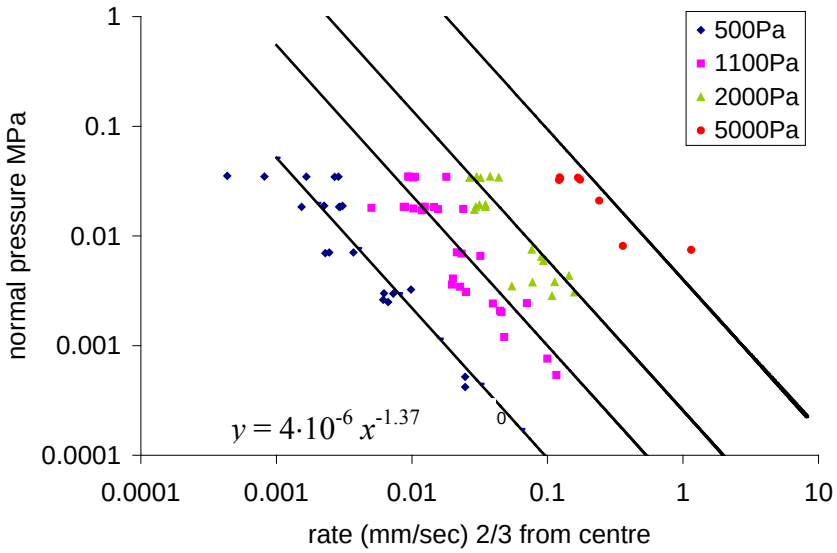

Fig. 10. Normal pressure versus rate data with trend lines of the form given in Eq (3) with C_2 = -1.37.

Fig 9 shows the data converted to normal pressure versus rate together with trend lines with C_2 = -1.37. The general form of the final master curve is assumed to take the form

$$P = C_3 \cdot a_\tau \cdot a_T \cdot v^{-1.37} \qquad (6)$$

where a_τ is the shift factor for the shear stress and a_T is the shift factor for the temperature. It is possible to shift the data horizontally, vertically or by a combination of the two methods, the choice here is arbitrary. A vertical shifting was chosen. In order to determine the shift factors a reference temperature and reference shear stress had to be chosen (180°C and 500Pa). Eq (6) could then be written as

$$P = 4 \times 10^{-6} \cdot a_\tau \cdot a_T \cdot v^{-1.37} \qquad (7)$$

when a_τ and a_T both equal 1, Eq (7) gives the trend line of the reference data, the lowest trend line shown in Fig 10. Thus the factor $4 \times 10^{-6} = C_{3ref}$ and includes the conversion from normal mass to normal pressure, i.e. C_{3ref} is the normal pressure measured in MPa that produces a velocity of

1mm/s at 2/3 of the platen radius from the centre of the platen under the reference conditions. The constant C_3 of each trend line can be related to C_3 of the reference curve, i.e., C_{3ref}, simply by determining the ratio between the two, as shown in see Eq (8). Thus a_τ is the factor by which the reference curve must be multiplied in order to shift it to coincide with trend lines fitted to data produced at other shear stresses at the reference temperature. Evidently the size of a_τ is determined by the relative magnitudes of the shear stresses of the two curves. A relationship of the form shown in Eq (8) is postulated. The aim is to determine the value of the exponent *b* in Eq (8). Table 3 shows the information used to determine *b*.

$$a_\tau = \frac{C_3}{C_{3ref}} = \left(\frac{\tau}{\tau_{ref}} \right)^b \tag{8}$$

Table 3. Information used to determine *b* in Eq (8)

Shear Stress (Pa)	C_3	$\frac{\tau}{\tau_{ref}}$	$\frac{C_3}{C_{3ref}}$	b
500	$4.0 \cdot 10^{-6}$	1	1	-
1100	$4.25 \cdot 10^{-5}$	2.2	10.65	3
2000	$2.56 \cdot 10^{-4}$	4	64	3
5000	$4.0 \cdot 10^{-3}$	10	1000	3

Here $\tau_{ref} = 500 \times 10^{-6}$ MPa, a value of $b = 3$ was determined from the data, thus Eq (6) can be written as

$$P = 4 \times 10^{-6} \cdot \left(\frac{\tau}{500 \times 10^{-6}} \right)^3 \cdot a_T \cdot v^{-1.37} \tag{9}$$

when $a_T = 1$ Eq (9) can be used to determine *P* at 180°C for shear stresses between 500 and 5000 Pa. A similar equation was determined for the other temperatures though the factor C_3 in each case was different. In order to apply Eq (9) to other temperatures all that remained was to determine a_T where

$$a_T = \frac{P(T)}{P(T_{ref})} = \frac{C_3(T)}{C_3(T_{ref})} \tag{10}$$

The relationship between a_T and temperature was assumed to follow an Arrhenius type behaviour, thus

$$\log(a_T) = A\left(\frac{1}{T} - \frac{1}{T_{ref}} \right) \tag{11}$$

The aim here is to determine *A*. This can be determined by plotting $\log(a_T)$ versus $(1/T - 1/T_{ref})$. Arrhenius type behaviour is indicated if the data follow a straight line. The data are plotted in Fig 11.

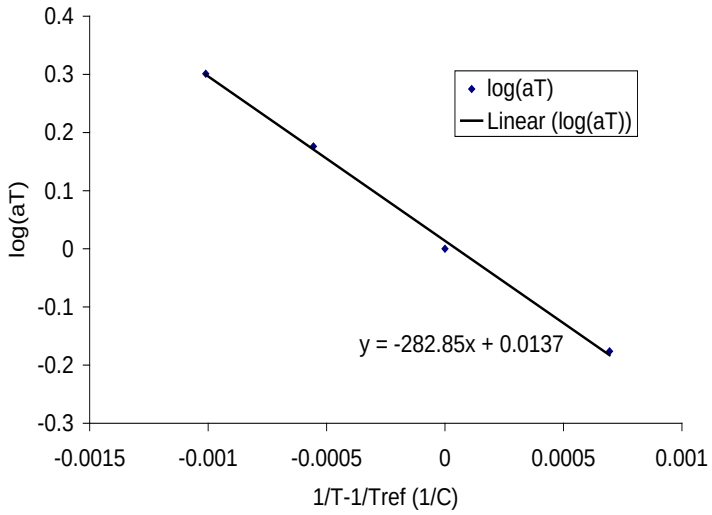

Fig 11. Determination of the gradient of the plotted data gives A in Eq (11)

A trend line fitted to the data gives A = -282.85. Thus, Eq (11) can be written

$$a_T = 10^{-282.85\left(\frac{1}{T}-\frac{1}{180}\right)} \tag{12}$$

and substituted in Eq (9) to produce a general equation including rate, normal pressure and temperature. However, the equation requires further modification. This is because a Newtonian assumption is made when the rheometer converts the intended input shear stress to torque for the parallel plate geometry [36]. This problem has been addressed for non-Newtonian fluids [37] resulting in Eq (13), which can be used to correct the friction data

$$\tau = \frac{M}{2\pi R^3}\left[3 + \frac{d\ln M}{d\ln v}\right] \tag{13}$$

where M is the applied torque. For a Newtonian fluid $d\ln M/d\ln v = 1$. For non-Newtonian fluid the term is less than 1. Using the rheometer data a value of approximately 0.39 was found. This results in a small modification to the Newtonian master curve, Eq (9) which can be rearranged as

$$\mu = 565\times10^{-6}\sqrt[3]{\frac{v^{1.37}}{4\times10^{-6}\cdot P^2\cdot a_T}} \tag{14}$$

where a_T is given by Eq (12) and μ it the coefficient of friction in N/N, v is the velocity in mm/s, P is the normal pressure in MPa and T is the temperature in ºC. Eq (14) will be referred to as the Master Curve in subsequent sections and is a purely empirical model. To permit comparison with experimental measurements and meso-scale model predictions, the master curve, Eq (14), has been used to generate results at specific experimental conditions, as noted in Table A3 (see Appendix A). Notably the experimental conditions chosen were within the working range of the rheometer.

4 STRIBECK ANALYSIS

The Stribeck curve has been used previously in several investigations to analyse the tool-ply friction of textiles composites [11, 13, 14, 16-18, 28, 30]. Values of 0.11 mm [17] and 0.07 mm [14, 25] have been employed in order to determine the shear rate in the fluid layer and calculate the matrix viscosity before plotting the data as a function of the Hersey number. A similar procedure is adopted here (see Fig 12) using a film thickness of 0.11mm. The experimental conditions of the data points are listed in Tables A1-3.

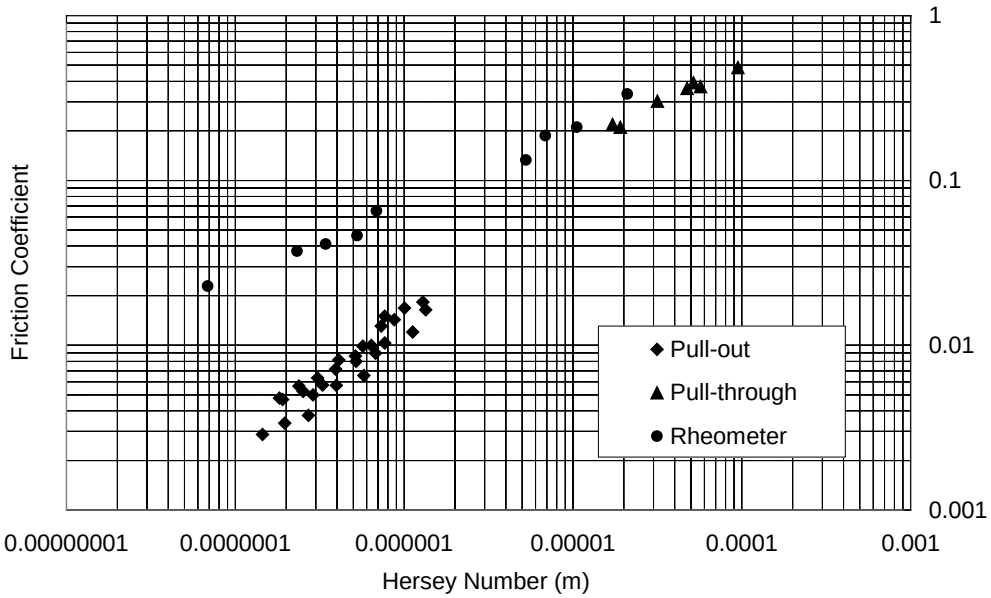

Fig 12. Coefficient of friction versus modified Hersey Number (m) using data from the literature. Pressure has been used to determine the Hersey number rather than normal force per meter or normal force.

The polypropylene matrix used in Twintex has been characterised previously and fitted with a Carreau-Yasuda model [38]. Using this information the viscosity of the fluid layer can be estimated. It should be noted that the rheological data measured in this characterisation were reliable only for relatively low shear rates ($<10s^{-1}$) which, when using a gap of 0.11mm, corresponds to a draw velocity of just $0.011mms^{-1}$. Above this the accuracy of the fitted Carreau-Yasuda model predictions become less certain but should still provide a reasonable estimate. As most of the investigations employed faster draw speeds, error in calculating the viscosity and hence the Hersey number is inevitable when plotting the data of Fig 12.

A clear trend in the data can be seen and shows that even for the very low Hersey numbers explored by Wilks [23] (achieved using low draw speeds combined with high normal pressures – see Table A1) the friction coefficient increases with Hersey number. Comparison with Fig 1 may therefore suggest full-film lubrication, a result which corresponds to that found by Gorczyca-Cole et al. [14] when conducting tests on Twintex fabric. However, data from the different tests fail to fall onto a single curve, indicating that the friction behaviour may be more complicated than can be described using a Stribeck analysis. A probable source of error in performing such an analysis is the use of a constant film thickness for all experimental conditions. Predictions from the meso-scale model described in Section 6 suggest the minimum film thickness can vary by several orders of magnitude according to the experimental conditions. Thus, one option in plotting the data is to use the film thickness predicted by the meso-scale model rather than use a constant film thickness. However, initial attempts by Ubbink [17] to do this failed to improve the data when interpreted using a Stribeck approach. Use of an alternative definition of the Hersey number used in this paper (compared to its original definition) may also be a source of error.

5 MESO-SCALE MODELLING

A meso-scale model [11, 17] based on a geometrical description of the tows within the fabric has been developed. One of the advantages of the model is that the film thickness can be predicted from the normal pressure and velocity. This avoids the use of the approximation of the film thickness required in the analysis of Section 5. Fig 13 presents a schematic cross section of the composite material in the warp direction. Hydrodyamic lubrication is assumed between the bundles and the tool surface. The total friction force per unit width follows by integrating the surface shear stresses over the length of the cross section, disregarding the bundle curvatures out of the plane for the time being. The contributions of the longitudinal warp and transverse weft yarns can be

analysed separately and added to calculate the total friction force and hence the friction coefficient. The Reynolds' equation describes the relation between the pressure and thickness distributions in thin film lubrication. The simple one dimensional steady state situation is given by

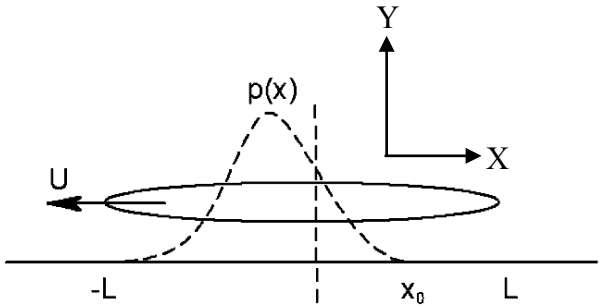

Fig. 13. Schematic pressure distribution underneath a bundle.

$$\frac{\partial}{\partial x}\left(\frac{h^3}{\eta}\frac{\partial P}{\partial x}\right) = 6v\frac{\partial h}{\partial x} \tag{15}$$

where v is the velocity, h is the film thickness in the Y direction and x is distance in the X direction (see Fig 13) and η is the viscosity predicted using the Carreau-Yasuda model fitted to the actual polypropylene viscosity data reported in [38]. Thus, the model is appropriate for predictions of steady state friction rather than the peak friction observed at the start of the test. The pressure distribution can be solved for a given film thickness distribution using the following boundary conditions (see Fig 13).

$$P(-L) = 0; \quad P(x_o) = 0; \quad \frac{\partial p}{\partial x}(x_o) = 0 \tag{16}$$

where the pressure is assumed to be non-negative. The bearing force per unit width is given by

$$F_B = \int_{-L}^{x_o} P(x)dx \tag{17}$$

whereas the friction force per unit width follows as

$$F_f = \int_{-L}^{x_o} \tau(x)dx = \int_{-L}^{x_o} \frac{h}{2}\frac{\partial P}{\partial x} + \eta\frac{v}{h}dx \tag{18}$$

The one dimensional meso-scale model predicts the bearing and friction forces, F_B and F_f, with the temperature T, velocity v and minimum film thickness h_{min} as input parameters. The model is used inversely, iteratively adapting h_{min} such that the integrated bearing force over all fibres equals the prescribed normal load N. This procedure also leads to the pull-out force, which can be converted to friction coefficient and compared to the experimental results. In order to compare the meso-scale model with the master curve given by Eq (14) the tow geometry within the fabric described in Section 2 must be modelled. The tow shape is characterised using a polynomial function, see Table 1 and Fig 2.

6 COMPARISON OF EXPERIMENTAL DATA WITH EMPIRICAL AND MESO-SCALE MODELS

The meso-scale model predicts a different minimum film thickness, h_{min}, for each experimental condition. This film thickness and the friction coefficient predicted by the meso-scale model are presented in Table A3. It was noted that for several experimental conditions the film thickness prediction was less than the yarn fibre diameter (16 microns) probably rendering the meso-scale model predictions invalid according to the underlying assumptions of the theory.

Nevertheless, friction predictions from the Master curve and meso-scale model are compared in Fig 14. A quantitative comparison can be drawn between the two using Eq (19).

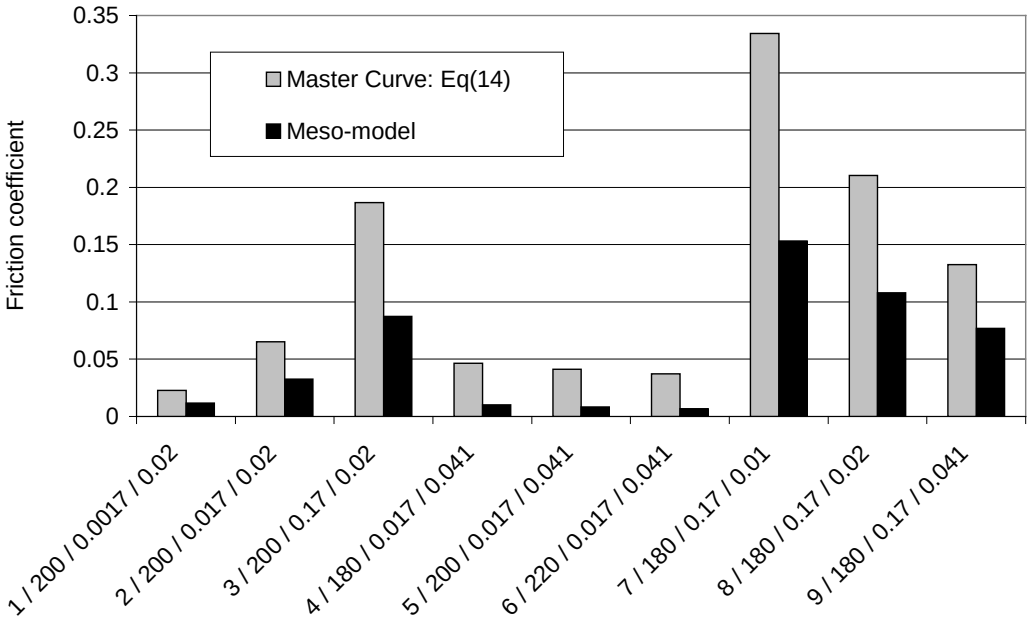

Fig 14. Comparison of Eq (14), indicated as Master Curve in the legend, with the meso-scale model. The experimental condition is given in the format of Number / Temperature (^{o}C) / Velocity (mm/s) / Pressure (MPa) to 2 significant figures.

$$relative\ error = \sum_{i=1}^{n} abs\left\{\frac{100\left(\mu_{MC} - \mu_{MSM}\right)}{\mu_{MC}}\right\} \Big/ m \tag{19}$$

where μ_{MC} is the master curve prediction for the friction coefficient and μ_{MSM} is the friction coefficient predicted using the meso-scale model, i is the number of the data value in a given set and m is the total number of data in the set. The meso-model correctly predicts the main trends in the data, though underestimates the friction by a factor of approximately two (for conditions where the film prediction is valid).

A comparison between the master curve and the experimental data produced using both pull-out and pull-through tests has also been attempted (see Tables A1 and A2). However, it was found that as it stands the master curve Eq (14) was unable to provide a close comparison. The reason for this is believed to be that normal forces and velocities used in collecting the rheometer data are very much lower than those used in conducting pull-though and pull-out tests which tend to be closer to actual forming conditions [30]. Thus, any error involved in the shifting process used to determine Eq (14) is magnified in extrapolating predictions to experimental conditions beyond the rheometer's working range. Thus, a modified version of Eq (14) is proposed:

$$\mu_{MMC} = K \cdot \mu_{MC} + G \tag{20}$$

where μ_{MC} is given by Eq (14) and two extra fitting parameters K and G have been introduced. They are easily determined by plotting the experimentally determined friction data against Eq (14) and fitting a linear trend-line using least squares (see Fig 15). The values of K and G for the two data sets given in Tables A1 and A2 are given in Fig 15.

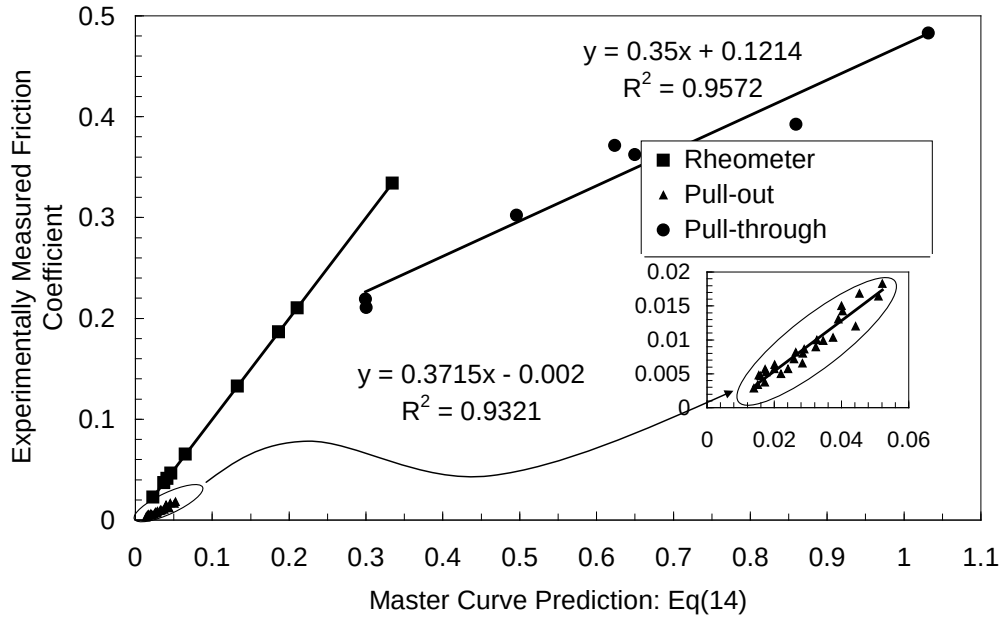

Fig 15. Friction coefficient versus Eq (14), pull-out and pull-through tests. Inset shows an expanded view of the pull-out data. Trendlines fitted to the data give the values of K and G in Eq (20). K = 0.3715, G = -0.002 for the pull-out data, K = 0.35, G = 0.1214 for the pull through data.

Finally, Fig 16 and Fig 17 s how a comparison between the pull-out and pull-through experimental data, the Modified Master Curve Eq (20) predictions and the meso-scale model predictions.

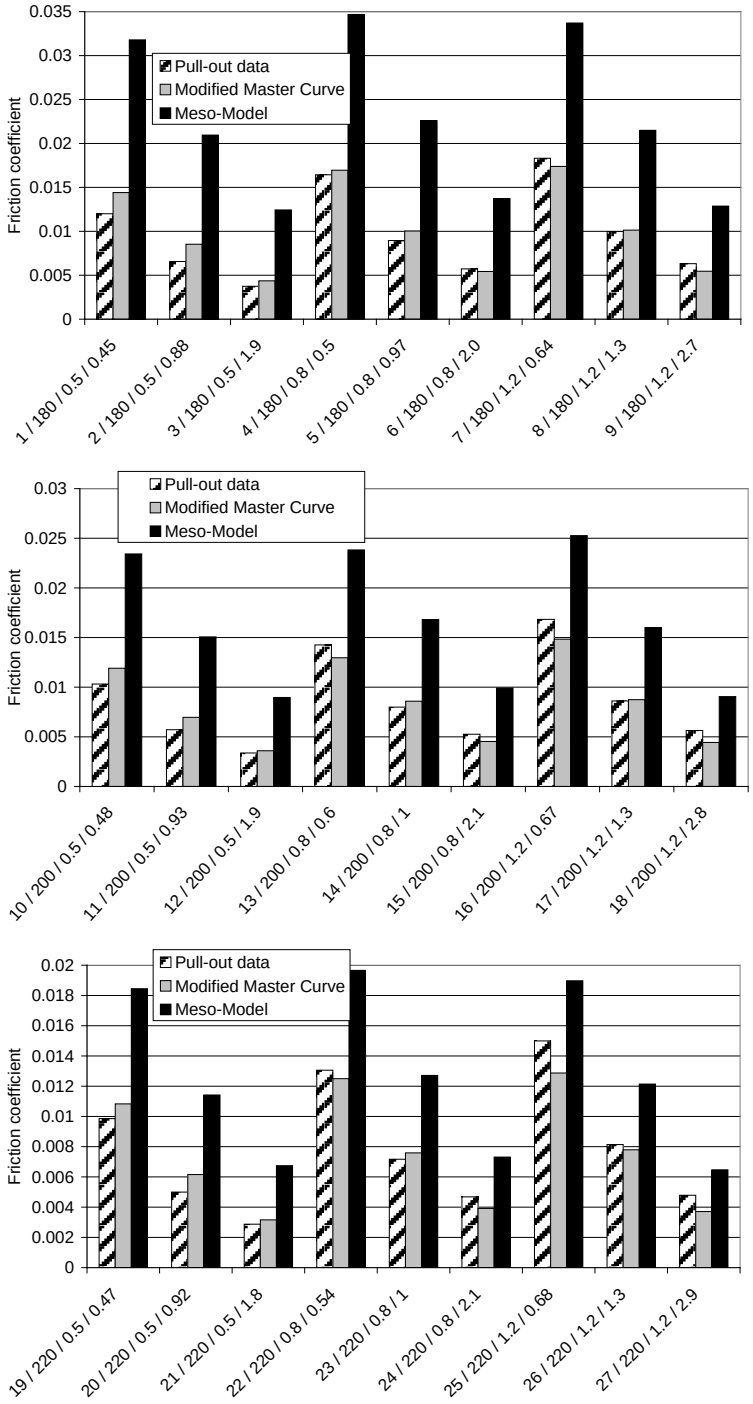

Fig 16. Comparison between pull-out data, the Modified Master Curve empirical model and Meso-Model Predictions. The experimental condition is given in the format of Number / Temperature (^{o}C) / Velocity (mm/s) / Pressure (MPa) to 2 significant figures.

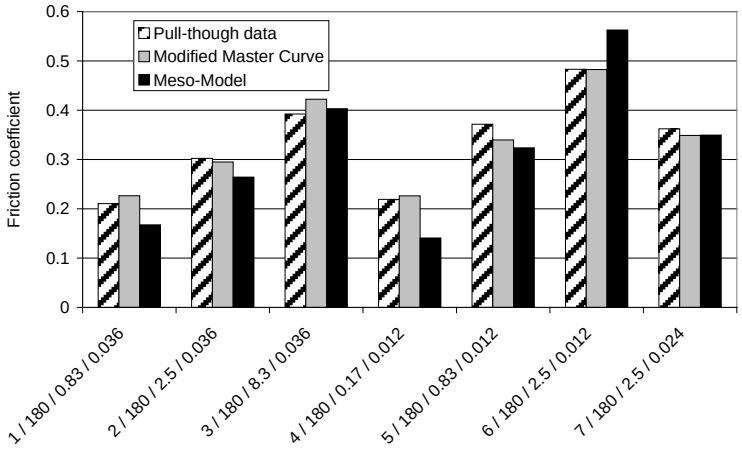

Figure 17. Comparison between pull-though data, Modified Master Curve empirical model and Meso-Model Predictions. The experimental condition is given in the format of Number / Temperature (^{o}C) / Velocity (mm/s) / Pressure (MPa) to 2 significant figures.

The average relative error expressed as a percentage for each comparison has been calculated using Eq (19).

7 CONCLUSIONS

As a final comment, Eq (15) is written in a form that is convenient for implementation in a finite element code. Implementation of this model will allow sensitivity studies to be conducted in order to assess the influence of pressure, velocity and temperature and hence the friction coefficient on the shear and wrinkling behaviour of the thermoplastic textile composite sheet during forming.

APPENDIX A

Table A1. Experimental conditions, pull-out friction measurement, Modified Master Curve friction prediction, minimum film thickness, h_{min}, and Meso-Scale Model friction prediction. The values marked with a * indicate that the film thickness predicted by the meso-model is less than the yarn fibre diameter, invalidating the meso-model friction prediction. Valid results are written in bold type.

Condition number	T (^{o}C)	v (mm/s)	P (MPa)	μ_{PO} Pull-out experiment	μ_{MMC} Modified Master Curve	h_{min} (mm)	μ_{MSM} Meso-Model
1	180	0.5	0.45	0.01200	0.01441	0.00705*	0.03179*
2	180	0.5	0.875	0.00656	0.00853	0.00227*	0.02095*
3	180	0.5	1.863	0.00375	0.00436	0.00050*	0.01243*
4	180	0.8	0.5	0.01643	0.01696	0.00845*	0.03468*
5	180	0.8	0.988	0.00895	0.01004	0.00267*	0.02260*
6	180	0.8	2.038	0.00573	0.00543	0.00063*	0.01373*
7	180	1.2	0.638	0.01831	0.01739	0.00767*	0.03371*
8	180	1.2	1.288	0.00998	0.01014	0.00223*	0.02150*
9	180	1.2	2.675	0.00632	0.00546	0.00050*	0.01287*
10	200	0.5	0.481	0.01032	0.01191	0.00311*	0.02342*
11	200	0.5	0.93	0.00572	0.00696	0.00087*	0.01506*
12	200	0.5	1.886	0.00337	0.00360	0.00019*	0.00896*
13	200	0.8	0.595	0.01426	0.01296	0.00310*	0.02383*
14	200	0.8	1	0.00799	0.00859	0.00113*	0.01681*
15	200	0.8	2.063	0.00526	0.00453	0.00024*	0.00991*
16	200	1.2	0.658	0.01683	0.01483	0.00353*	0.02527*
17	200	1.2	1.291	0.00862	0.00874	0.00095*	0.01601*
18	200	1.2	2.785	0.00564	0.00444	0.00018*	0.00905*
19	220	0.5	0.468	0.00985	0.01083	0.00158*	0.01845*
20	220	0.5	0.924	0.00500	0.00616	0.00039*	0.01142*
21	220	0.5	1.835	0.00288	0.00316	0.00008*	0.00675*
22	220	0.8	0.538	0.01306	0.01250	0.00179*	0.01966*
23	220	0.8	1	0.00717	0.00759	0.00050*	0.01271*
24	220	0.8	2.063	0.00468	0.00392	0.00010*	0.00731*
25	220	1.2	0.684	0.01500	0.01287	0.00156*	0.01898*
26	220	1.2	1.278	0.00814	0.00780	0.00042*	0.01214*
27	220	1.2	2.873	0.00479	0.00371	0.00007*	0.00647*

Table A2. Experimental conditions, pull-through friction measurement, Modified Master Curve friction prediction, minimum film thickness, h_{min}, and Meso-Scale Model friction prediction. The values marked with a * indicate that the film thickness predicted by the meso-model is less than the yarn fibre diameter, invalidating the meso-model friction prediction. Valid results are written in bold type.

Condition number	T (^{o}C)	v (mm/s)	P (MPa)	μ_{pt} Pull-Through Experiment	μ_{MMC} Modified Master Curve	h_{min} (mm)	μ_{MSM} Meso-Model
1	**180**	**0.833**	**0.036**	**0.21055**	**0.22653**	**0.11577**	**0.16748**
2	**180**	**2.5**	**0.036**	**0.30232**	**0.29503**	**0.18305**	**0.26435**
3	**180**	**8.33**	**0.036**	**0.39237**	**0.42229**	**0.26218**	**0.40319**
4	**180**	**0.167**	**0.012**	**0.21922**	**0.22626**	**0.09334**	**0.14077**
5	**180**	**0.83**	**0.012**	**0.37156**	**0.33968**	**0.21461**	**0.32374**
6	**180**	**2.5**	**0.012**	**0.48303**	**0.48256**	**0.33440**	**0.56271**
7	**180**	**2.5**	**0.024**	**0.36227**	**0.34892**	**0.23203**	**0.34955**

Table A3. Experimental conditions, Master Curve friction prediction, minimum film thickness, h_{min}, and Meso-Scale Model friction prediction. The values marked with a * indicate that the film thickness predicted by the meso-model is less than the fibre diameter, invalidating the meso-model friction prediction. Valid results are written in bold type.

Condition number	T (^{o}C)	v (mm/s)	P (MPa)	μ_{MC} Master Curve	h_{min} (mm)	μ_{MSM} Meso-Model
1	200	0.00167	0.02037	0.0228	0.00087*	0.01161*
2	200	0.01667	0.02037	0.0652	0.00792*	0.03255*
3	**200**	**0.16667**	**0.02037**	**0.1866**	**0.05007**	**0.08749**
4	180	0.01667	0.04074	0.0463	0.00066*	0.01021*
5	200	0.01667	0.04074	0.0411	0.00043*	0.00827*
6	220	0.01667	0.04074	0.0372	0.00028*	0.00675*
7	**180**	**0.16667**	**0.01019**	**0.3342**	**0.10284**	**0.15320**
8	**180**	**0.16667**	**0.02037**	**0.2105**	**0.06699**	**0.10782**
9	**180**	**0.16667**	**0.04074**	**0.1326**	**0.04115**	**0.07684**

REFERENCES

1. Kalpakjian, S.S., S., *Manufacturing Engineering and Technology*. 2006, Pearson Prentice Hall.
2. Chenot, J.L., *State of the art and recent developments in the numerical modeling of metal forming processes*, in *9th International ESAFORM Conference on Materials Forming*. 2005: Cluj-Napoca, Romania. p. 71-76.
3. Lin, H., Long, A.C., Clifford, M.J., Wang, J. & Harrison, P., *Predictive Modelling of FE Forming to Determine Optimum Processing Conditions*, in *10th International ESAFORM Conference on Materials Forming*. 2007: Zaragosa, Spain. p. 1092-1097.
4. Lin, H., Wang, J., Long, A.C., Clifford, M.J. & Harrison, P., *Predictive Modelling for Optimisation of Textile Composite Forming.* Composites Science and Technology, 2007. **67**: p. 3242-3252.
5. Dong, L., Lekakou, C. & Bader, M. G., *Solid-mechanics finite element simulations of the draping of fabrics: a sensitivity analysis.* Composites Part A: Applied Science and Manufacturing, 2000. **31**(7): p. 639-652.
6. Morris, S.R., & Sun, C.T., *An investigation of interply slip behaviour in AS4/PEEK at forming temperatures.* Composites Manufacturing, 1994. **5**(4): p. 217-224.
7. Phung, T., Paton, R., & Mouritz, P.A., *Characterisation of interply shearing resistance of carbon-epoxy unidirectional tape and fabric prepregs*, in *6th International ESAFORM Conference on Materials Forming*. 2003: Salerno, Italy. p. 867-870.
8. Scherer, R., & Friedrich, K., *Inter- and intraply-slip flow processes during thermoforming of CF/PP-laminates.* Composites Manufacturing, 1991. **2**(2): p. 92-96.
9. Martin, C.J., Seferis, J.C., and Wilhelm M.A., *Frictional resistance of thermoset prepregs and its influence on honeycomb composite processing.* Comp. Part A, 1996. **27**(10): p. 943-951.
10. Lebrun, G., Bureau, M.N. & Denault, J., *Thermoforming-stamping of continuous glass fibre / PP composites: Interlaminar and tool-laminate shear properties.* Journal of Thermoplastic Composite Materials, 2004. **17**: p. 137-165.
11. Akkerman, R., Ubbink, M.P., de Rooij, M.B., & ten Thije, R.H.W. *Tool-ply friction in composite forming*. in *10th International ESAFORM Conference on Materials Forming*. 2007. Zaragosa, Spain.
12. Gorczyca, J.L., Sherwood, J.A. & Chen, J., *Friction between the tool and the fabric during the thermostamping of woven co-mingled glass-polypropylene composite fabrics*, in *Am Soc Comp 18th Tech. Conf.* 2003: Gainesville, FL.
13. Gorczyca, J.L., Sherwood, J.A. & Chen, J., *A friction model for use with a commingled glass-polypropylene plane weave fabric and the metal tool during thermostamping.* Revue Europeeanne des Elements Finis, 2005: p. 729-751.
14. Gorczyca-Cole, J.L., Sherwood, J.A. & Chen, J., *A friction model for thermostamping commingled glass-polypropylene woven fabrics.* Composites Part A, 2007. **38**: p. 393-406.
15. Harrison, P., Lin, H., Ubbink, M., Akkerman, R., van de Haar, K. & Long, A.C., *Characterising and Modelling Tool-Ply Friction of Viscous Textile Composites*, in *16th International Conference on Composite Materials*. 2007: Kyoto, Japan.
16. ten Thije, R.H.W.A., R., van der Meer, L. & Ubbink, M.P., *Tool-ply friction in thermoplastic composite forming*, in *11th International ESAFORM Conference on Materials Forming*. 2008: Lyon, France.
17. Ubbink, M., *Tool ply friction of woven fabric composites*, in *Mechanical Engineering*. 2006, University of Twente.
18. Van de Haar, K., *Modelling resistance at the ply/tool contact interface for Twintex®.* 2005, University of Nottingham.
19. Lin, H., Harrison, P., Van de Haar, K., Wang, J., Long, A.C., Akkerman, R. & Clifford, M.J. *Investigation of Tool-Ply Friction of Textile Composites*. in *8th International Conference on Textile Composites (TEXCOMP)*. 2006. Nottingham, UK.

20. Wilks, C.E., *Processing technologies for woven glass polypropylene composites*. 1999, University of Nottingham.
21. Murtagh, A.M., Lennon, J.J. & Mallon, P.J., *Surface friction effects related to pressforming of continuous fibre thermoplastic composites.* Composites Manufacturing, 1995. **6**: p. 169-175.
22. Murtagh, A.M., Monaghan, M.R. & Mallon P.J., *Investigation of the Interply Slip Process in Continuous Fibre Thermoplastic Composites*, in *9th ICCM*. 1993: University of Zaragoza, Spain. p. 311-318.
23. Wilks, C.E., Rudd, C.D., Long, A.C. & Johnson, C.F., *Tool/Ply Friction and Consolidation during Processing of Glass/Thermoplastic Composites*, in *6th International Conference on Automated Composites*. 1999: Bristol, UK
24. Gorczyca-Cole, J.L., Sherwood, J.A., Liu, L. & Chen, J., *Modeling of Friction and Shear in Thermostamping of Composites - Part I.* Journal of Composite Materials, 2004. **38**(21): p. 1911-1929.
25. Gorczyca-Cole, J.L., Sherwood, J.A. & Chen, J., *A friction model for use with a commingled glass-polypropylene plane weave fabric and the metal tool during thermostamping.* Revue Europeeanne des Elements Finis, 2005: p. 729-751.
26. Lussier, D.S., Chow, S. & Chen, J., *Shear and Friction Response of Co-Mingled Glass/Polypropylene Fabrics During Stamping*, in *American Society for Composites 16th Technical Conference*. 2001: Blacksburg, VA.
27. Heyer, P., & Lauger, J. *A flexible platform for tribological measurements on a rheometer*. in *15th International Congress on Rheology/80th Annual Meeting of the Society-of-Rheology*. 2008. Monterey, CA: Amer Inst Physics.
28. Chow, S., *Frictional interaction between blank holder and fabric in stamping of woven thermoplastic composites*, in *Department of Mechanical Engineering*. 2002, University of Massachusetts: Lowell.
29. Gorczyca-Cole, J.L., Sherwood, J.A. & Chen, J., *Friction between the tool and the fabric during the thermostamping of woven co-mingled glass-polypropylene composite fabrics*, in *Am Soc Comp 18th Tech. Conf.* 2003: Gainesville, FL.
30. Gorczyca, J.L., Sherwood, J.A., Liu, L. & Chen, J., *Modeling of Friction and Shear in Thermostamping of Composites - Part I.* Journal of Composite Materials, 2004. **38**(21): p. 1911-1929.
31. Clifford, M.J., Long, A.C. & deLuca, P., *Forming of engineering prepregs and reinforced thermoplastics*, in *TMS annual meeting and exhibition, second global symposium on innovations in materials, processing and manufacturing: sheet materials: composite processing*. 2001: New Orleans, LA.
32. Hutchings, I.M., *Tribology: Friction and Wear of Engineering Materials*. 1992, London: Edward Arnold. 273.
33. Kumar, P.C., Menezes, P.L. & Kailas, S.V., *Role of Surface Texture on Friction under Boundary Lubricated Conditions.* Tribology Online, 2008. **3**(1): p. 12-18.
34. Lee, J., et al., *Enhancement of lubrication properties of nano-oil by controlling the amount of fullerene nanoparticle additives.* Tribology Letters, 2007. **28**(2): p. 203-208.
35. Harrison, P., Clifford, M.J., Long, A.C. and Rudd, C.D., *Constitutive modelling of impregnated continuous fibre reinforced composites: Micromechanical approach.* Plastics, Rubber and Composites, 2002. **31**(2): p. 76-85.
36. Bohlin Instruments, L., *User Manual for Bohlin Rheometers*. 2001. p. 183.
37. Darby, R., *Viscoelastic Fluids; An Introduction to Their Properties and Behaviour*. in Chemical Processing and Engineering 1976, New York and Basel: Marcel Dekker.
38. Harrison, P., Clifford, M.J., Long, A.C. & Rudd, C.D., *A constituent-based predictive approach to modelling the rheology of viscous textile composites.* Composites: Part A, 2004. **35**: p. 915-931.